Journal of Power Sources 196 (2011) 3729–3735

Contents lists available at ScienceDirect

Journal of Power Sources

journal homepage: www.elsevier.com/locate/jpowsour

Double-perovskites $YBaCo_{2-x}Fe_xO_{5+\delta}$ cathodes for intermediate-temperature solid oxide fuel cells

Jingfeng Xue, Yu Shen, Tianmin He*

State Key Laboratory of Superhard Materials, and College of Physics, Jilin University, Changchun 130012, PR China

ARTICLE INFO

Article history:
Received 15 November 2010
Received in revised form
16 December 2010
Accepted 16 December 2010
Available online 24 December 2010

Keywords:
Solid oxide fuel cell
Double perovskite
Cathode
Electrical conductivity
Thermal expansion
Electrochemical performance

ABSTRACT

Double-perovskites $YBaCo_{2-x}Fe_xO_{5+\delta}$ (YBCF, $x = 0.0$, 0.2, 0.4 and 0.6) are synthesized with a solid-state reaction and are assessed as potential cathode materials for utilization in intermediate-temperature solid oxide fuel cells (IT-SOFCs) on the $La_{0.9}Sr_{0.1}Ga_{0.8}Mg_{0.115}Co_{0.085}O_{2.85}$ (LSGMC) electrolyte. The YBCF materials exhibit chemical compatibility with the LSGMC electrolyte up to a temperature of 950 °C. The conductivity of the YBCF samples decreases with increasing Fe content, and the maximum conductivity of YBCF is 315 S cm^{-1} at 325 °C for the $x = 0.0$ sample. A semiconductor–metal transition is observed at about 300–400 °C. The thermal expansion coefficient of the YBCF samples increases from 16.3 to 18.0 $\times 10^{-6}$ K^{-1} in air at temperatures between 30 and 900 °C with increase in Fe content. The area-specific resistances of YBCF cathodes at $x = 0.0$, 0.2 and 0.4 on the LSGMC electrolyte are 0.11, 0.13 and 0.15 Ω cm^2 at a temperature of 700 °C, respectively. The maximum power densities of the single cells fabricated with the LSGMC electrolyte, $Ce_{0.8}Sm_{0.2}O_{1.9}$ (SDC) interlayer, NiO/SDC anode and YBCF cathodes at $x = 0.0$, 0.2 and 0.4 reach 873, 768 and 706 mW cm^{-2}, respectively. This study suggests that the double-perovskites YBCF ($0 \le x \le 0.4$) can be potential candidates for utilization as IT-SOFC cathodes.

© 2010 Elsevier B.V. All rights reserved.

1. Introduction

Solid oxide fuel cells (SOFCs) have received considerable attention because of the advantages of their use, such high energy-conversion efficiency, low pollution and extensive fuel flexibility. The traditional SOFCs need high temperatures to function (typically at ~1000 °C), which can cause complex material-related issues and increase high fabrication costs of the cell system. Lowering the operating temperatures of the SOFCs down to an intermediate-temperature (IT) range of 600–800 °C not only can expand the choice of materials but also can reduce the costs involved in developing such as cell system. This increases the reliability and durability of the SOFC system operation. However, the polarization losses of the cathodes dramatically increase with decreasing operating temperatures of the SOFCs. Therefore, it is very important to develop cathode materials that have high electrocatalytic activity for use in the IT-SOFCs [1–3]. Much effort has been expended to develop high-performance simple-perovskite cathodes for the IT-SOFCs. Some of the representative materials tested so far can be briefly listed as follows: lanthanide cobaltite-based cathodes [4–7], A-site cation occupied by alkaline earth cobaltite [8], lanthanide ferrite-based cathodes [9,10], nickelates [11] and cuprates [12]. For further details on the development of cathode materials for IT-SOFCs, including research on the above mentioned cathode materials, recent in-depth reviews can be consulted [2,13–16].

In recent times, oxygen-deficient double-perovskites $LnBaCo_2O_{5+\delta}$ (Ln = La, Pr, Nd, Sm, Gd and Y) have been developed as potential cathode materials for use in IT-SOFCs because of their high oxygen vacancy concentration, adequate electrical conductivity and consequent excellent cathode performance [17–39]. In this new family of cathodes, the double-perovskite $LnBaCo_2O_{5+\delta}$ from Ln = Pr to Gd have been systemically studied, with the exception of the Ln = La sample which has no oxygen vacancy in the perovskite lattice at room temperature [22]. However, there is minimal information on the use of $YBaCo_2O_{5+\delta}$ as a cathode for IT-SOFCs [30]. Kim and Manthiram reported that the $YBaCo_2O_{5+\delta}$ cathode had a lower thermal expansion coefficient (TEC), but was compromised by interfacial reaction with the $La_{0.8}Sr_{0.2}Ga_{0.8}Mg_{0.2}O_{2.8}$ (LSGM) electrolyte after being heated at 1000 °C for 3 h [22]. Zhang et al. reported that the $YBaCo_2O_{5+\delta}$ sample was stable at 850 °C for 100 h in air, but became unstable at 850 °C for 100 h in a reducing nitrogen atmosphere [24]. Therefore, the chemical stability and compatibility of the $YBaCo_2O_{5+\delta}$ cathode appears to be largely dependent on the temperature and atmosphere. It is also seen that no reaction products could be observed in the $YBaCo_2O_{5+\delta}$ and $La_{0.9}Sr_{0.1}Ga_{0.8}Mg_{0.115}Co_{0.085}O_{2.85}$ (LSGMC) mixtures after calcining at 950 °C for 2 h, as reported in a previous work by these authors that is described in the present paper; this implies that the use of $YBaCo_2O_{5+\delta}$ as a cathode material in IT-SOFCs is feasible.

* Corresponding author. Tel.: +86 431 85166112; fax: +86 431 85166112.
E-mail addresses: hetm@jlu.edu.cn, hly@mail.jlu.edu.cn (T. He).

0378-7753/$ – see front matter © 2010 Elsevier B.V. All rights reserved.
doi:10.1016/j.jpowsour.2010.12.071

Similar to other perovskite cobaltite cathodes, the double-perovskite cathodes $LnBaCo_2O_{5+\delta}$ had high TECs, which ranged from $24.3 \times 10^{-6}\,K^{-1}$ for Ln = La to $16.6 \times 10^{-6}\,K^{-1}$ for Ln = Gd at temperatures between 80 and 900 °C in air, whereas the TEC for the Ln = Y double-perovskite was $15.8 \times 10^{-6}\,K^{-1}$ under the same conditions [22]. Liu reported that the average TEC of the sample for Ln = Y was $14.5 \times 10^{-6}\,K^{-1}$ at temperatures between 200 and 800 °C [30]. This indicates that the double-perovskite $YBaCo_2O_{5+\delta}$ had the lowest TEC, which placed it closer to the IT-electrolytes (e.g., the TEC of GDC electrolyte was $12.4–12.5 \times 10^{-6}\,K^{-1}$ between 30 and 1000 °C in air [14,40]). From the point of view of thermal expansion compatibility, similar TECs between the cathode and the electrolyte are required to mitigate significant strain caused by thermal cycling and to improve their adherence to the electrolytes. In addition, the substitution of a low-cost iron with chemical properties similar to cobalt on the B-site of the $YBaCoO_{5+\delta}$ would further reduce the costs of developing cobalt-containing cathode materials. Therefore, in this article, we systemically investigated the properties, including phase structure, chemical compatibility, electrical conductivity, TEC and electrochemical impedance, of $YBaCo_{2-x}Fe_xO_{5+\delta}$ (YBCF, x = 0.0, 0.2, 0.4 and 0.6) as cathodes of IT-SOFCs. The performance of LSGMC electrolyte-supported cells with SDC as the interlayer, NiO/SDC as the anode and YBCF (x = 0.0, 0.2 and 0.4) as cathode was also tested at various temperatures.

2. Experimental data

2.1. Sample preparation

The $YBaCo_{2-x}Fe_xO_{5+\delta}$ (YBCF, x = 0.0, 0.2, 0.4 and 0.6) samples were synthesized using a conventional solid-state reaction. Samples for the composition of YBCF were prepared by mixing commercial powders of Y_2O_3 (99.9%), $BaCO_3$ (99.5%), Co_3O_4 (99%) and Fe_2O_3 (99.5%) in stoichiometric proportions. The mixtures were ground in an agate mortar for 1 h, and then pressed into pellets and calcined at 1000 °C for 12 h. The calcined samples were pulverized and reground, and, subsequently, the powders were uniaxially pressed into pellets (13 mm in diameter and 1 mm thickness) and cylinders (6 mm in diameter and thickness 5–6 mm) at 220 MPa for electrical conductivity and thermal expansion measurements. Finally, the compacted pellets and cylinders were sintered at 1100 °C for 20 h in air, and then cooled to room temperature at a cooling rate of 100 °C h^{-1}. Samples of LSGMC, SDC and NiO powders were prepared by the glycine nitrate process [41,42].

2.2. Characterization

The crystal structure and chemical compatibility of the samples were identified using a high-power X-ray diffractometer (Rigaku-D-Max γA, Cu-Kα radiation, λ = 0.15418 nm, 12 kW), with an angle size of 0.02° and scanning range of 20–80° at room temperature. A scanning electron microscope (SEM; JEOL JSM-6480LV) was used to inspect the microstructures of sintered samples. Conductivity measurements were performed on sintered pellets at temperatures ranging from room temperature to 850 °C in air using the van der Pauw method that utilizes a DC standard voltage/current generator (SB118) and a precision digital multimeter (PZ158A). Thermal expansion measurements were carried out between 30 and 900 °C in air using a push-rod dilatometer (Netzsch DIL 402C) with an Al_2O_3 reference at a heating rate of 5 °C min^{-1}, and the flow rate of air was maintained at 60 mL min^{-1}. For cell fabrication, electrolyte-supported symmetrical electrochemical cells and single-cell SOFCs were prepared to evaluate the electrochemical performances of the YBCF cathodes. LSGMC, with a fixed thickness of 300 μm each, was used as the electrolyte and NiO/SDC (in a weight ratio of 65:35) was used as the anode. For symmetrical cells, the cathode paste was applied on both sides of the LSGMC electrolyte pellets and calcined at 950 °C for 2 h. Electrochemical impedance spectroscopy of the symmetrical cells was measured from 700 to 800 °C with 50 °C increments in air using an electrochemical analyzer (CHI604C) with a frequency range of 0.1–100 kHz and an AC amplitude of 10 mV. For single cells, to prevent reaction at the anode/electrolyte interface, an SDC interlayer was first prepared by screen-printing onto the anode side of the LSGMC electrolyte and sintered at 1300 °C for 1 h. Single cells with the configuration of NiO-SDC/SDC/LSGMC/YBCF were applied for electrochemical performances studies. The anode was sintered at 1250 °C for 4 h in air. Silver paste was used to attach silver meshes as the current collector onto the electrode surfaces [26]. Tests of single-cell performance were conducted with the anode under dry H_2 and the cathode in ambient air over a temperature range of 650–800 °C with intervals of 50 °C.

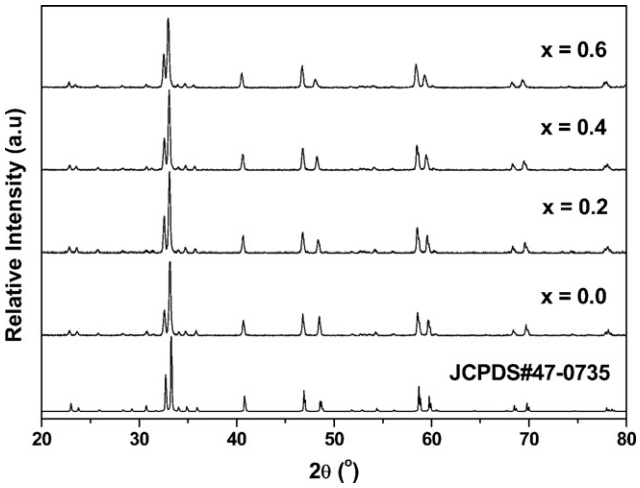

Fig. 1. XRD patterns of the YBCF samples sintered at 1100 °C for 20 h in air: (a) JCPDS#47-0735, (b) x = 0.0, (c) x = 0.2, (d) x = 0.4 and (e) x = 0.6.

3. Results and discussion

3.1. XRD analysis and chemical compatibility

Fig. 1 depicts X-ray diffraction (XRD) patterns of the samples YBCF (x = 0.0, 0.2, 0.4 and 0.6) after sintering at 1100 °C for 20 h in air. All of the YBCF compositions were identified as single-phase double-perovskites. There were no secondary phases detected in the sintered samples. In Fig. 1, it can be seen that the main XRD peaks of the YBCF sample shift gradually toward the low-angle direction with increasing Fe content. This indicates that the lattice expansion increases with increase in doping content of larger ion-radius Fe^{3+} in cobalt-sites. The crystal structure of these YBCF samples can be indexed as a tetragonal structure, which has also been reported by other researchers [22,30,43–45]. Zhang et al. [24] demonstrated that $YBaCo_2O_{5+\delta}$ crystallized as an orthorhombic structure. This structural disagreement mainly originated due to the differing oxygen content in the perovskite lattices. In a report by Akahoshi and Ueda [46], the phase structure of the $YBaCo_2O_{5+\delta}$ was detailed to be very sensitive to the oxygen content in the lattices. Samples of $YBaCo_2O_{5+\delta}$ with $\delta \geq 0.50$ were orthorhombic structures; samples with $0.25 \leq \delta \leq 0.44$ were tetragonal structures; and samples with $0.00 \leq \delta \leq 0.19$ could either be orthorhombic or tetragonal primitive cells when crystallized. Therefore, it is logical that $YBaCo_2O_{5+\delta}$ would crystallize with different structures with differences of oxygen content in the samples.

It is well known that the phase reaction between the electrode and electrolyte is detrimental for the durability of an SOFC oper-

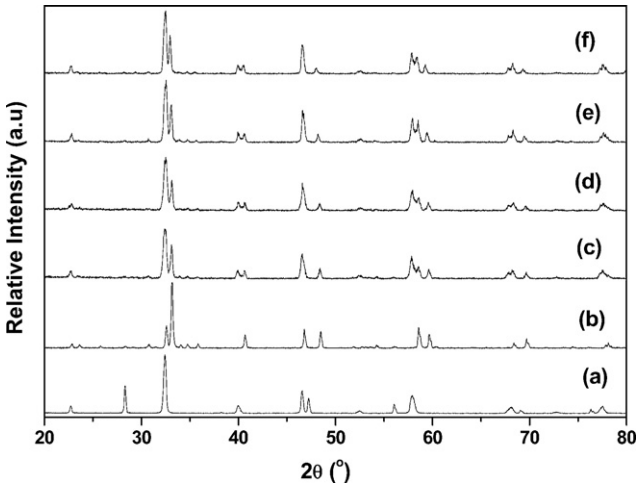

Fig. 2. XRD patterns of the YBCF and LSGMC mixtures sintered at 950 °C for 2 h in air: (a) LSGMC powders, (b) YBCF powders for $x = 0.0$, (c) YBCF–LSGMC mixtures for $x = 0.0$, (d) YBCF–LSGMC mixtures for $x = 0.2$, (e) YBCF–LSGMC mixtures for $x = 0.4$ and (f) YBCF–LSGMC mixtures for $x = 0.6$.

ation. Kim and Manthiram reported that $YBaCo_2O_{5+\delta}$ suffers an interfacial reaction with the LSGM electrolyte when sintered at 1000 °C for 3 h, and this limits its use as a cathode in SOFCs [22]. To examine the chemical compatibility between YBCF electrodes and LSGMC electrolytes, X-ray diffraction measurements were obtained for a mixture of YBCF and LSGMC powders in a 1:1 weight ratio that was sintered at 950 °C for 2 h (Fig. 2). For comparison, the XRD patterns of the $YBaCo_2O_{5+\delta}$ and LSGMC powders have also been included in Fig. 2. It is clear from XRD data that there were no undesired reactions between YBCF cathodes and the LSGMC electrolyte, and no marked shifts were detected for the XRD peaks in these patterns. This indicates that the YBCF double-perovskites when used as cathodes are chemically compatible with the LSGMC electrolyte up to a temperature of 950 °C. The structural stability of the $YBaCo_2O_{5+\delta}$ in air was also confirmed by annealing the sample at 850 °C for 100 h [24], and this implies that $YBaCo_2O_{5+\delta}$-based materials are structurally stable and chemically compatible with the LSGMC electrolyte in air.

Table 1 presents data calculated for lattice parameters and unit-cell volumes of the YBCF samples. The lattice parameter value for $x = 0.0$ in this study accords well with those reported by other researchers [22,44,45]. We note that lattice parameters and unit-cell volumes increase with increase in Fe content. The ionic radii of the Co^{3+}/Co^{4+} and Fe^{3+}/Fe^{4+} are 0.061/0.053 and 0.0645/0.0585 nm, respectively, in six-coordination [47]. Therefore, lattice parameters and unit-cell volumes of the YBCF are expected to increase with the substitution of Fe for Co because the ionic radius of Fe is greater than that of Co. Similar trends have been observed in Fe-doped $YBaCo_2O_{5+\delta}$, $TbBaCo_2O_{5.5}$ and $NdBaCo_2O_{5+\delta}$ systems by other researchers [43,48,49].

3.2. Microstructure and electrical conductivity

Fig. 3 presents SEM micrographs of surface views of the YBCF samples sintered at 1100 °C for 20 h in air. The average grain sizes of the YBCF samples decrease and the porosities increase with increase in Fe content. Further, pore sizes among grains increase progressively. Disk-shaped grains are observed in the samples for both $x = 0.4$ and 0.6. Observation of the SEM microstructure

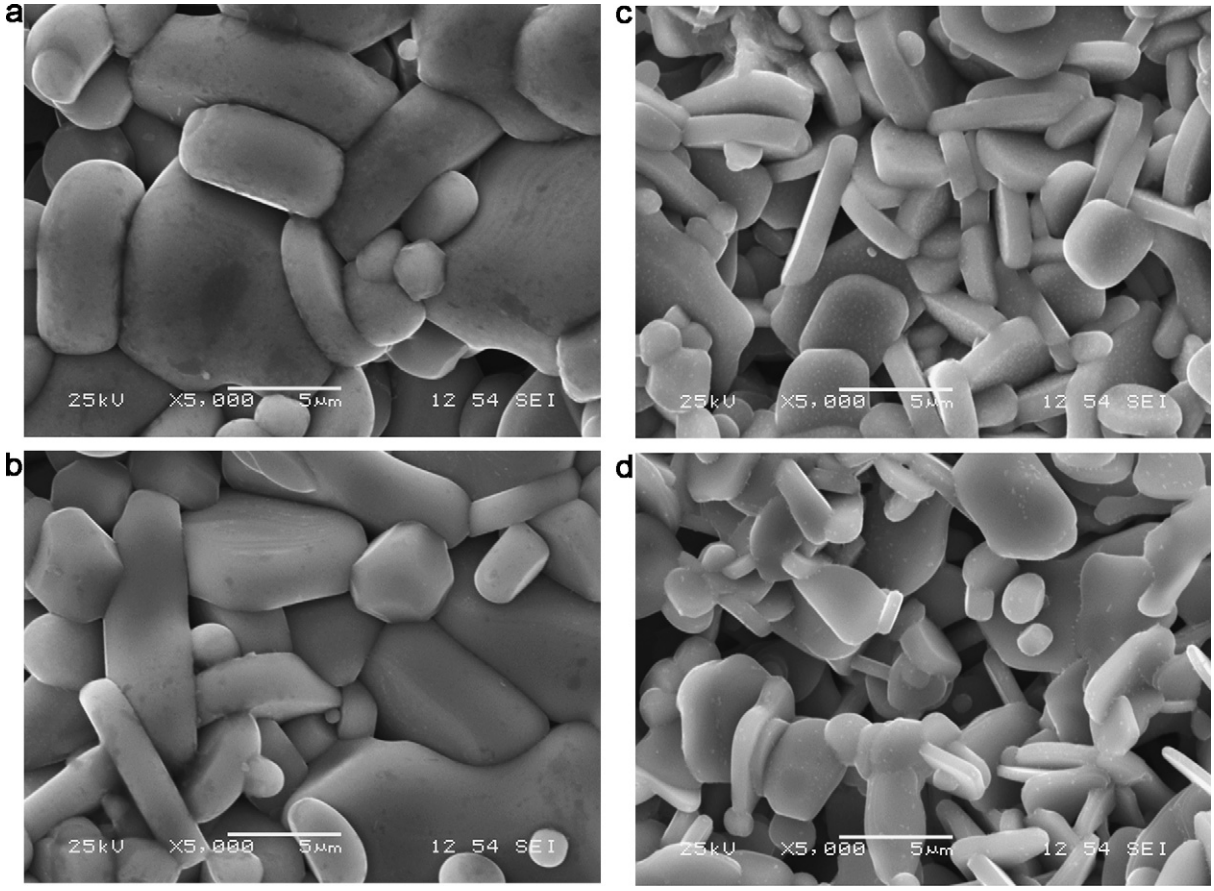

Fig. 3. SEM micrographs for the surface views of YBCF pellets: (a) $x = 0.0$, (b) $x = 0.2$, (c) $x = 0.4$ and (d) $x = 0.6$.

Table 1
Structural parameters, TEC, ASR on the LSGMC and activation energy of the YBCF oxides.

Sample	Structural parameters			ASR (Ω cm^2)			TEC $\times 10^{-6}$ (K^{-1})	Activation energy (eV)
	a (Å)	c (Å)	V (Å^3)	800 °C	750 °C	700 °C		
X = 0.0	3.8790	7.5089	112.98	0.061	0.083	0.11	16.3	0.49
X = 0.2	3.8807	7.5186	113.23	0.071	0.094	0.13	17.3	0.52
X = 0.4	3.8853	7.5347	113.74	0.082	0.11	0.15	18.0	0.53
X = 0.6	3.8933	7.5552	114.52					

indicates that sintered densities of YBCF samples decrease with increase in Fe content. This accords well with the electrical conductivity analysis in the following section.

Fig. 4 depicts the electrical conductivity of YBCF samples at a range of temperatures from room temperature to 850 °C in air, when measured by the van der Pauw four-probe method. A semiconductor–metal transition occurred at about 300–400 °C. Conductivities of YBCF samples gradually increased with increasing temperatures, and this represents a semiconductor-like behavior. These samples achieve their respective maximums between 325 and 425 °C with change from x = 0.0 to 0.6 and, then, begin to decrease, exhibiting a metal-like characteristics. Similar behaviors were also reported in a study of the $LnBaCo_{2-x}Fe_xO_{5+\delta}$ (Ln = Nd and Gd) double-perovskites [49]. With thermogravimetric analysis (TGA), Zhang et al. demonstrated that the oxygen commenced release from the lattices in YBCF samples beyond temperatures of about 300 °C [43] and this formed the oxygen vacancies in lattices. Kim et al. reported that this change occurred beyond 200 °C for $LnBaCo_{2-x}Fe_xO_{5+\delta}$ (Ln = Nd and Gd) systems [49]. The formation of oxygen vacancies is accompanied by a reduction of high-valence-state Co^{4+} to Co^{3+}, and a resultant decrease of the carrier concentration and Co–O covalence for the p-type semiconductor [26]. Therefore, the electrical conductivity of YBCF samples can be said to decrease after about 300 °C. In addition, oxygen vacancies in lattices perturb the (Co, Fe)–O–(Co, Fe) periodic potential and covalent interaction [50]. This constitutes another reason for the decreased electrical conductivity of YBCF samples at high temperatures. Based on the above analysis, the apparent semiconductor–metal transition can be attributed to the reduction in valence from Co^{4+} to Co^{3+} [51] and the release of oxygen from lattices [43].

The electrical conductivity of YBCF samples decreases markedly with increase in Fe content. It has been reported in a TGA study that oxygen vacancies increased with increasing Fe content [43]. For a p-type semiconductor of YBCF compositions, Co^{4+} ions constitute the majority of carriers [50]. The oxygen and Co^{4+} ion content in YBCF samples decreases with increasing Fe content, and leads to the reduction of the carrier concentration and, consequently, this results in decreased electrical conductivity. The decrease in conductivity with increase in Fe content was also reported for the $LnBaCo_{2-x}Fe_xO_{5+\delta}$ (Ln = Nd and Gd) systems [49]. The maximum conductivity of the YBCF sample for x = 0.6 at 425 °C is almost one order of magnitude lower than that of the $YBaCo_2O_{5+\delta}$ sample at 325 °C, which is only 34 S cm^{-1}. Therefore, other properties of the sample for x = 0.6 have not been included in the following section as its conductivity is too low.

3.3. Thermal expansion behavior

Fig. 5 characterizes linear thermal expansion curves of YBCF samples that are measured between 30 and 900 °C in air. The average TEC value of these samples are 16.3×10^{-6}, 17.3×10^{-6} and 18.0×10^{-6} K^{-1} for x = 0.0, 0.2 and 0.4, respectively. These TEC values are lower than those of certain cobalt-containing cathodes, such as $Sm_{0.5}Sr_{0.5}CoO_3$ [6], $La_xSr_{1-x}Fe_yCo_{1-y}O_{3-\delta}$ [7], $LnBaCo_2O_{5+\delta}$ (Ln = Nd, Sm, and Gd) [22,52] and $SrCo_{1-y}Nb_yO_{3-\delta}$ [53]. In comparison with other cobalt-containing cathodes, YBCF oxides offer a better thermal expansion match to the intermediate-temperature electrolytes such as LSGM and LSGMC [7,42,54]. TEC values of these YBCF samples increased gradually with increase in Fe content. In general, the TEC is smaller for the smaller unit-cell for the same crystal structure, because the binding energy between ions in the lattice increased with decreasing ion distance [55]. In Table 1, unit-cell volumes of YBCF samples increase with increasing Fe content, and, consequently, the TECs increase.

Fig. 6 presents differential curves of $\Delta L/L_o$ against temperature for YBCF samples at temperatures between 30 and 900 °C. An abrupt change can be observed in these differential curves, indicating that electronic phase transitions exist in YBCF sam-

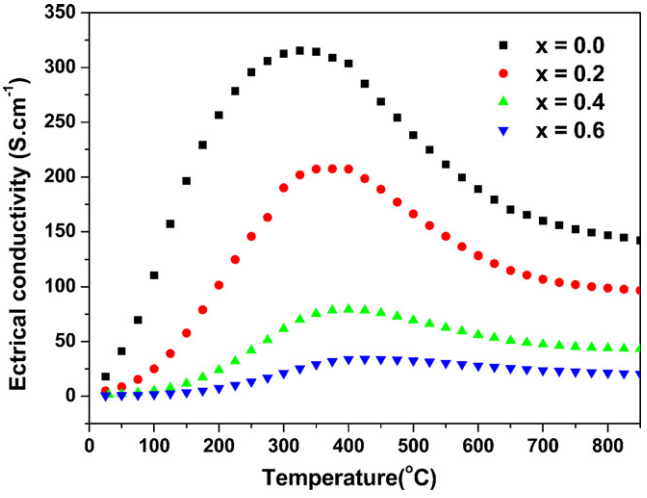

Fig. 4. Temperature dependence of the electrical conductivity of the YBCF samples: (a) x = 0.0, (b) x = 0.2, (c) x = 0.4 and (d) x = 0.6.

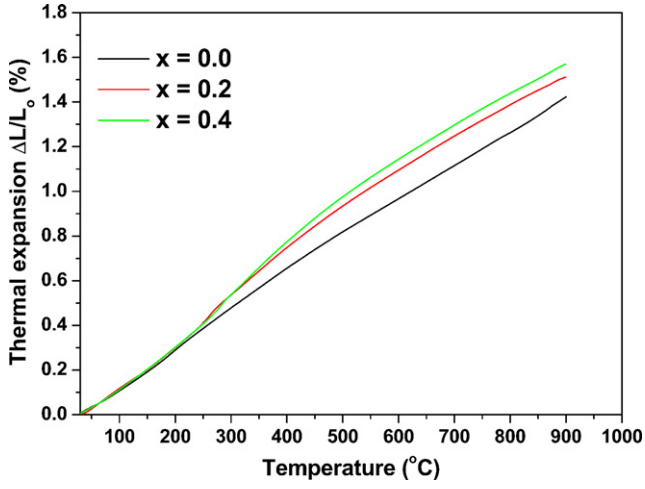

Fig. 5. Thermal expansion curves of the YBCF samples between 30 and 900 °C in air: (a) x = 0.0, (b) x = 0.2 and (c) x = 0.4.

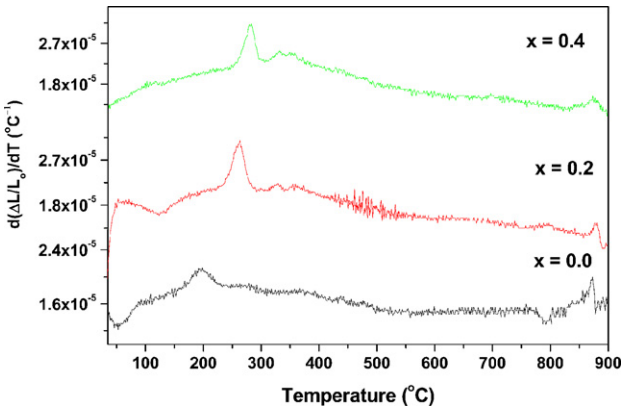

Fig. 6. Differential curves of $\Delta L/L_o$ against temperature for the samples YBCF in air: (a) $x = 0.0$, (b) $x = 0.2$ and (c) $x = 0.4$.

ples, wherein the Co^{4+} reduces to Co^{3+} and the oxygen in lattices is released to generate oxygen vacancy. This concurs with TGA results that have been reported by other researchers [43,49,51]. The phase-transition temperature shifts gradually toward higher temperatures as compared with $YBaCo_2O_{5+\delta}$, indicating that the phase-transition temperature increases with increasing Fe content. This is mainly attributed to the fact that the Fe–O bond is stronger than the Co–O bond and inhibits oxygen loss when YBCF samples are heated [49], and, therefore, increase in phase-transition temperatures are observed in samples proportional to increasing Fe content.

3.4. AC-impedance measurement

A symmetrical cell arrangement was used to measure the AC impedance of cathodes on a LSGMC electrolyte. Fig. 7 depicts the typical impedance spectra for a YBCF cathode at $x = 0.0$ that is measured at various temperatures (700, 750 and 800 °C) in air. Similar AC-impedance spectra are also observed for both $x = 0.2$ and $x = 0.4$ samples. In these impedance spectra, the interception with the real axis at low frequencies represents a total resistance of the symmetrical cell, and the value of intercept at high frequencies is a total ohmic resistance, which encompasses electrolyte, electrode ohmic, lead and contact resistances between cell and current collector [56]. The difference between these two intercept values corresponds with the polarization resistance (or area-specific resistance (ASR)), which is the sum of the resistances of the two cathode–electrolyte

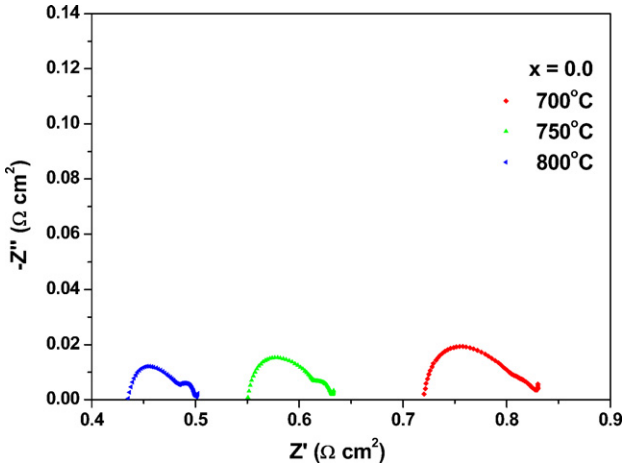

Fig. 7. Typical impedance spectra of the YBCF cathode at $x = 0.0$ on the LSGMC electrolyte measured at 700–800 °C in air.

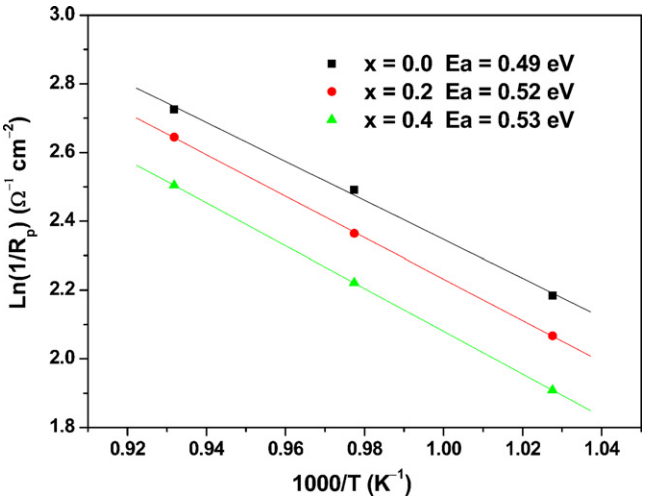

Fig. 8. Arrhenius plots of the ASR values for the YBCF cathodes ($0 \le x \le 0.4$).

interfaces. Therefore, the original ASR values in the impedance spectra were divided by two to obtain the interfacial resistance of the cathode–electrolyte combination. Two depressed arcs are depicted in impedance spectra for all samples in the temperature range of 700–800 °C, and these arcs correspond with at least two different electrode processes. The arc in the high-frequency range represents the transfer of oxygen ions from the electrode into the electrolyte and the arc in the low-frequency range is attributed to a combination of oxygen adsorption/desorption, surface/bulk diffusion and gas-phase diffusion processes [57]. The target value of the ASR for a cathode is lower than 0.15 Ω cm^2 at the operating temperature [58,59]. Values characterizing the evolution of the ASR for YBCF ($x = 0.0$, 0.2 and 0.4) cathodes with the corresponding temperature and x values are listed in Table 1. It can be seen that ASRs of YBCF cathodes on LSGMC electrolytes are 0.11, 0.13 and 0.15 Ω cm^2 at 700 °C, which meets the requirement of the cathode with regard to the ASR. The ASRs of YBCF cathodes on the LSGMC electrolyte are higher as compared with those of $LnBaCo_2O_{5+\delta}$ (Ln = Pr, Nd, Sm and Gd) cathodes [52]. Taskin et al. reported that bulk-diffusion and surface exchange coefficients of $LnBaCo_2O_{5+\delta}$ materials decreased with decrease of the Ln^{3+} ion radii from Pr to Ho [60]. The Y^{3+} ion radius is lower than that of the Ln^{3+} ion from Pr to Ho [47]. Therefore, ASRs of YBCF cathodes are higher than those of $LnBaCo_2O_{5+\delta}$ cathodes (Ln = Pr, Nd, Sm and Gd). Moreover, the ASR of the YBCF cathodes increases with increasing Fe content. This is primarily due to Co possesses higher electrocatalytic property for oxygen reduction than Fe.

Fig. 8 presents Arrhenius plots of ASR values for YBCF cathodes on the LSGMC electrolyte. From the slope of the fitted line, activation energies are calculated as 0.49, 0.52 and 0.53 eV for $x = 0.0$, 0.2 and 0.4 samples on the LSGMC electrolyte, respectively.

3.5. Performance of single-cell

Fig. 9 depicts the variation of cell voltage and power density as a function of current density for NiO-SDC/SDC/LSGMC/YBCF cells using H_2 as the fuel and ambient air as the oxidant in a temperature range of 650–800 °C, respectively. The maximum power densities of the cells reach 873, 768 and 706 mW cm^{-2} at 800 °C for $x = 0.0$, 0.2 and 0.4 cathodes, respectively. There is good accord between the measured AC impedance and the performance of the single-cell. Higher cell performances are mainly attributed to better sintering performance, adequate electrical conductivity, smaller TEC and lower ASR of the YBCF on the LSGMC electrolyte. In addition, the maximum power densities of cells with the $YBaCo_2O_{5+\delta}$

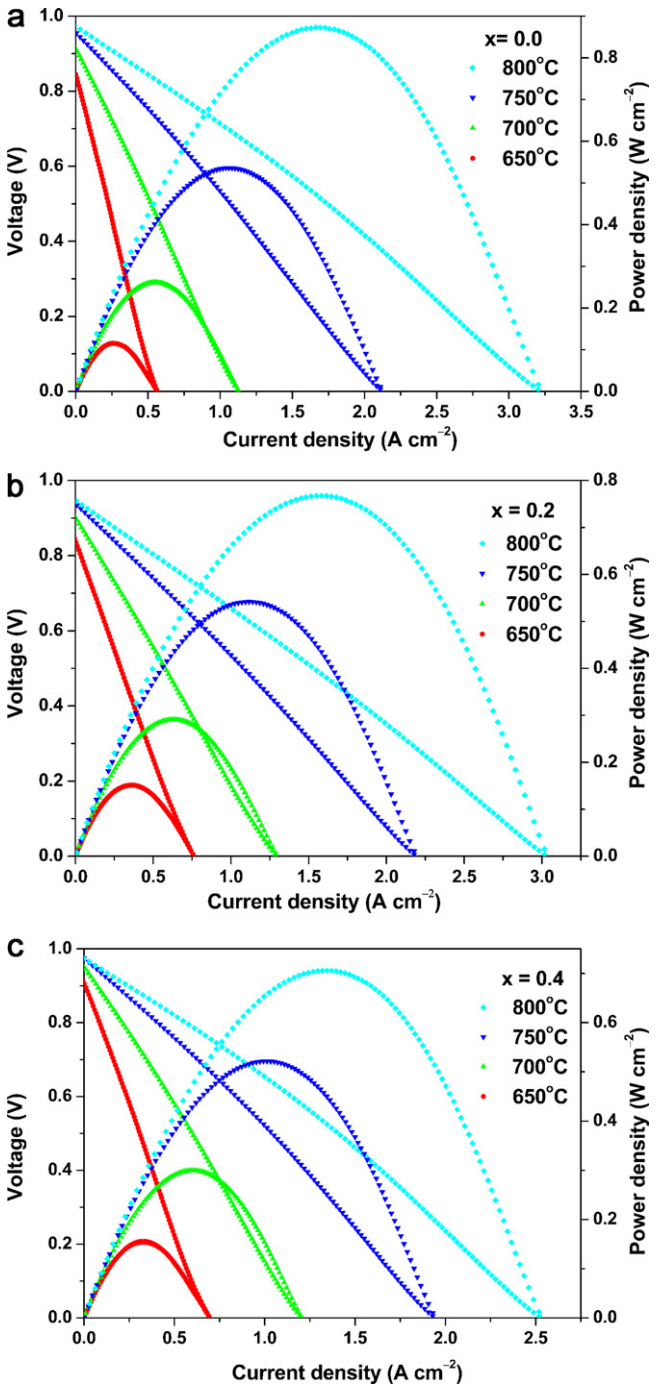

Fig. 9. Electrochemical performance data of the NiO-SDC/SDC/LSGMC/YBCF single cells using dry H_2 as fuel and ambient air as oxidant in the temperature range of 600–800 °C: (a) $x = 0.0$, (b) $x = 0.2$ and (c) $x = 0.4$.

cathode were higher than those of cells with the $SmBaCo_2O_{5+\delta}$ cathode, as reported previously [26]. This finding can be elucidated with regard to the different electrolytes used, wherein the conductivity of the LSGM electrolyte was 6.06×10^{-2} S cm^{-1} at 800 °C [41] and that of the LSGMC electrolyte was 9.40×10^{-2} S cm^{-1} at 800 °C [42]. The high performance of YBCF cathodes is particularly attractive with regard to IT-SOFCs. However, the degradation on long-term performance of a cell with YBCF cathodes has not been completely investigated here. Further research is necessary to determine the long-term stability of cells that have YBCF as a cathode.

4. Conclusions

The double-perovskite YBCF ($x = 0.0$, 0.2, 0.4 and 0.6) were assessed systemically as potential cathode materials of IT-SOFCs. The unit-cell volumes of YBCF cathodes increase with increasing Fe content. The YBCF cathodes demonstrate good chemical compatibility with the LSGMC electrolyte at temperatures up to 950 °C. All samples exhibited a semiconductor–metal transition at temperatures of about 300–400 °C. The conductivity of YBCF cathodes decreased with increase in Fe content, whereas the average TECs and ARSs of YBCF cathodes increased. The ASRs of the YBCF cathodes were 0.11, 0.13 and 0.15 Ω cm^2 at 700 °C for $x = 0.0$, 0.2 and 0.4, respectively. The maximum power densities of single cells with $x = 0.0$, 0.2 and 0.4 cathodes reached values of 873, 768 and 706 mW cm^{-2} at 800 °C, respectively. From a combined perspective of economic consideration and good cell performance, YBCF cathodes with $x = 0.2$ and 0.4 appear to be more suited for application in IT-SOFCs. By applying changes such as the use of the cobalt-containing electrolyte material LSGMC instead of LSGM and by lowering the calcining temperature of cathodes on electrolyte, the interfacial reaction between cathode and electrolyte can be avoided effectively. Although further research is necessary to evaluate degradation with long-term performance in the cell with YBCF cathodes, preliminary indications vouch positive for the application of YBCF cathodes in IT-SOFCs, and imply that YBCF oxides could have potential in application as cathode materials for IT-SOFCs.

Acknowledgement

This work was supported by the Natural Science Foundation of China under contract no. 10974065.

References

[1] S.P. Jiang, J. Mater. Sci. 43 (2008) 6799–6833.
[2] E.V. Tsipis, V.V. Kharton, J. Solid State Electrochem. 12 (2008) 1367–1391.
[3] D.J.L. Brett, A. Atkinson, N.P. Brandon, S.J. Skinner, Chem. Soc. Rev. 37 (2008) 1568–1578.
[4] B.C.H. Steele, J.M. Bae, Solid State Ionics 106 (1998) 255–261.
[5] H. Fukunaga, M. Koyama, N. Takahashi, C. Wen, K. Yamada, Solid State Ionics 132 (2000) 279–285.
[6] S. Yang, T.M. He, Q. He, J. Alloys Compd. 450 (2008) 400–404.
[7] H. Ullmann, N. Trofimenko, F. Tietz, D. Stöver, A. Ahmad-Khanlou, Solid State Ionics 138 (2000) 79–90.
[8] Z. Shao, S.M. Haile, Nature 431 (2004) 170–173.
[9] S.P. Simner, J.F. Bonnett, N.L. Canfield, K.D. Meinhardt, V.L. Sprenkle, J.W. Stevenson, Electrochem. Solid State Lett. 5 (2002) A173–A175.
[10] A. Mai, V.A.C. Haanappel, S. Uhlenbruck, F. Tietz, D. Stöver, Solid State Ionics 176 (2005) 1341–1350.
[11] G. Amow, S.J. Skinner, J. Solid State Electrochem. 10 (2006) 538–546.
[12] Q. Li, H. Zhao, L. Huo, L. Sun, X. Cheng, J.C. Grenier, Electrochem. Commun. 9 (2007) 1508–1512.
[13] C. Sun, R. Hui, J. Roller, J. Solid State Electrochem. 14 (2010) 1125–1144.
[14] A. Tarancón, M. Burriel, J. Santiso, S.J. Skinner, J.A. Kilner, J. Mater. Chem. 20 (2010) 3799–3813.
[15] A.J. Jacobson, Chem. Mater. 22 (2010) 660–674.
[16] A. Orera, P.R. Slater, Chem. Mater. 22 (2010) 675–690.
[17] A.M. Chang, S.J. Skinner, A. Kilner, Solid State Ionics 177 (2006) 2009–2011.
[18] A. Tarancón, S.J. Skinner, R.J. Chater, F. Hernández-Ramírez, J.A. Kilner, J. Mater. Chem. 17 (2007) 3175–3181.
[19] A. Tarancón, A. Morata, G. Dezanneau, S.J. Skinner, J.A. Kilner, S. Estradé, F. Hernández-Ramírez, F. Peiró, J.R. Morante, J. Power Sources 174 (2007) 255–263.
[20] G. Kim, S. Wang, A.J. Jacobson, L. Reimus, P. Brodersen, C.A. Mims, J. Mater. Chem. 17 (2007) 2500–2505.
[21] N. Li, Z. Lü, B. Wei, X.Q. Huang, K.F. Chen, Y.H. Zhang, W.H. Su, J. Alloys Compd. 454 (2008) 274–279.
[22] J.-H. Kim, A. Manthiram, J. Electrochem. Soc. 155 (4) (2008) B385–390.
[23] B. Lin, S.Q. Zhang, L.C. Zhang, L. Bi, H.P. Ding, X.Q. Liu, J.F. Gao, G.Y. Meng, J. Power Sources 177 (2008) 330–333.
[24] K. Zhang, L. Ge, R. Ran, Z.P. Shao, S.M. Liu, Acta Mater. 56 (2008) 4876–4889.
[25] C. Zhu, X. Liu, C. Yi, D. Yan, W. Su, J. Power Sources 185 (2008) 193–196.
[26] Q.J. Zhou, T.M. He, Y. Ji, J. Power Sources 185 (2008) 754–758.

[27] A. Tarancón, J. Peña-Martínez, D. Marrero-López, A. Morata, J.C. Ruiz-Morales, P. Núñez, Solid State Ionics 179 (2008) 2372–2378.
[28] J. Peña-Martínez, A. Tarancón2, D. Marrero-López, J.C. Ruiz-Morales, P. Núñez, Fuel Cells 8 (5) (2008) 351–359.
[29] J.-H. Kim, F. Prado, A. Manthiram, J. Electrochem. Soc. 155 (10) (2008) B1023–B1028.
[30] Y. Liu, J. Alloys Compd. 477 (2009) 860–862.
[31] D. Chen, R. Ran, K. Zhang, J. Wang, Z. Shao, J. Power Sources 188 (2009) 96–105.
[32] H. Gu, H. Chen, L. Gao, Y. Zheng, X. Zhu, L. Guo, Int. J. Hydrogen Energy 34 (2009) 2416–2420.
[33] B. Lin, Y. Dong, R. Yan, S. Zhang, M. Hu, Y. Zhou, G. Meng, J. Power Sources 186 (2009) 446–449.
[34] J.H. Kim, A. Manthiram, Electrochim. Acta 54 (2009) 7551–7557.
[35] J.H. Kim, Y. Kim, P.A. Connor, J.T.S. Irvine, J. Baea, W. Zhou, J. Power Sources 194 (2009) 704–711.
[36] L. Zhao, B. He, Z. Xun, H. Wang, R. Peng, G. Meng, X. Liu, Int. J. Hydrogen Energy 35 (2010) 753–756.
[37] J.H. Kim, M. Cassidy, J.T.S. Irvine, J. Bae, Chem. Mater. 22 (2010) 883–892.
[38] H.P. Ding, X.J. Xue, J. Alloys Compd. 496 (2010) 683–686.
[39] H.P. Ding, X.J. Xue, Electrochim. Acta 55 (2010) 3812–3816.
[40] Y.C. Zhang, Q.J. Zhou, T.M. He, J. Power Sources 196 (2011) 76–83.
[41] L.G. Cong, T.M. He, Y. Ji, P.F. Guan, Y.L. Huang, W.H. Su, J. Alloys Compd. 348 (2003) 325–331.
[42] J.F. Xue, Y. Shen, Q.J. Zhou, T.M. He, Y.H. Han, Int. J. Hydrogen Energy 35 (2010) 294–300.
[43] X.T. Zhang, H.S. Hao, X. Hu, Physica B 403 (2008) 3406–3409.
[44] W. Zhou, Chem. Mater. 6 (1994) 441–447.
[45] A. McKinlay, P. Connor, J.T.S. Irvine, W. Zhou, J. Phys. Chem. C 111 (51) (2007) 19120–19125.
[46] D. Akahoshi, Y. Ueda, J. Solid State Chem. 156 (2001) 355–363.
[47] R.D. Shannon, Acta Crystallogr. A32 (1976) 751–767.
[48] M. Kopcewicz, D.D. Khalyavin, I.O. Troyanchuk, H. Szymczak, R. Szymczak, D.J. Logvinovich, E.N. Naumovich, J. Appl. Phys. 93 (2003) 479–486.
[49] Y.N. Kim, J.-H. Kim, A. Manthiram, J. Power Sources 195 (2010) 6411–6419.
[50] H. Takahashi, F. Munakata, M. Yamanaka, Phys. Rev. B 57 (1998) 15211–15218.
[51] L.-W. Tai, M.M. Nasrallah, H.U. Anderson, D.M. Sparlin, S.R. Sehlin, Solid State Ionics 76 (1995) 259–271.
[52] Q.J. Zhou, F. Wang, Y. Shen, T.M. He, J. Power Sources 195 (2010) 2174–2181.
[53] F. Wang, Q.J. Zhou, T.M. He, G.D. Li, H. Ding, J. Power Sources 195 (2010) 3772–3778.
[54] V.V. Kharton, F.M.B. Marques, A. Atkinson, Solid State Ionics 174 (2004) 135–149.
[55] H. Hayashi, M. Watanabe, M. Ohuchida, H. Inaba, Y. Hiei, T. Yamamoto, M. Mori, Solid State Ionics 144 (2001) 301–313.
[56] H. Lv, Y.-J. Wu, B. Huang, B.-Y. Zhao, K.-A. Hu, Solid State Ionics 177 (2006) 901–906.
[57] S.-W. Baek, J.H. Kim, J. Bae, Solid State Ionics 179 (2008) 1570–1574.
[58] B.C.H. Steele, Solid State Ionics 86–88 (1996) 1223–1234.
[59] B.C.H. Steele, A. Heinzel, Nature 414 (2001) 345–352.
[60] A.A. Taskin, A.N. Lavrov, Y. Ando, Prog. Solid State Chem. 35 (2007) 481–490.